Tentative Structures for the Radiation-Induced Radicals in Crystalline β-D-Fructose Using Density Functional Theory

Ewald Pauwels,*,† Philippe Lahorte,‡ Gauthier Vanhaelewyn,§ Freddy Callens,§ Frank De Proft,|| Paul Geerlings,|| and Michel Waroquier†

Laboratory of Theoretical Physics, Ghent University, Proeftuinstraat 86, B-9000 Gent, Belgium, European Patent Office, Bayerstrasse 34, D-80335 Munich, Germany, Department of Solid State Sciences, Ghent University, Krijgslaan 281-S1, B-9000 Gent, Belgium, and Eenheid Algemene Chemie (ALGC), Free University of Brussels, Pleinlaan 2, B-1050 Brussels, Belgium

Received: July 1, 2002; In Final Form: October 8, 2002

In this study, density functional theory calculations were used to identify the structure of the radiation-induced radicals in solid state β-D-fructose, using a single molecule approach. Four model radicals were proposed, and the electron paramagnetic resonance (EPR) parameters were calculated for the optimized geometries. These calculated parameters were subsequently compared with those of two radical species, observed in an experimental EPR and electron nuclear double resonance study on irradiated fructose (Vanhaelewyn, G.; Lahorte, P.; De Proft, F.; Mondelaers, W.; Geerlings, P.; Callens, F. *Phys. Chem. Chem. Phys.* **2001**, *3*, 1729). On the basis of this preliminary comparison, three model structures were rejected. By varying the main degree of freedom of the remaining model, a number of conformations were obtained that yielded isotropic and anisotropic hyperfine tensor components in close agreement with experimental results. To disentangle between these possible conformers, a detailed study was made of the hyperfine tensor eigenvectors. One conformation was found to be in close agreement with the experimental measurement of the hyperfine tensor of the two observed radical species. It was concluded that these experimental species are in fact manifestations of one and the same radical, with a structure conforming to our model but with slightly altered conformations.

1. Introduction

Saccharides play an essential role in most biological processes. They are extremely abundant in plants and are vital in the biological energy storage and transport systems of animals. The simple sugars D-fructose and D-glucose are of particular interest in this respect, since they are the monomeric units of the disaccharide sucrose, one of the most widespread sugars in nature.

In recent years, considerable attention has been given to radiation-induced free radicals in solid state sugars, in light of the radiation treatment of sugar-containing food. This treatment improves the hygienic quality, as ionizing radiation sterilizes and reduces the bioburden. From the safety and regulatory point of view, identification of irradiated food and determination of irradiation doses are a major concern. This has spawned research into the development of dosimetric protocols for the various foodstuffs that are suitable for radiation treatment. In this respect, electron paramagnetic resonance (EPR) spectroscopy might be one of the most reliable methods to detect irradiation, because of the relative stability of radiation-induced radicals in certain foodstuffs. The presence of these radicals constitutes a suitable probe for the irradiation doses. Dosimetric protocols have already been established for a number of foodstuffs (e.g., bone-containing[1] and cellulose-containing food[2]), but a protocol for sugar-containing foods is still in the developmental stage. A number of studies are available that focus on the overall dosimetric characteristics and the ensuing applications of the sugar system.[3] Other studies have focused rather on trying to understand on a fundamental level the nature of the sugar EPR spectra by elucidating the identity and structural characteristics of the radicals involved. For this purpose, sucrose has been examined using EPR techniques under various experimental conditions, such as (frozen) solution,[4] powders,[5] and single crystals.[6−8] Up to now, however, no unambiguous identification has been made of the radiation-induced radicals present in solid state sucrose. Gräsland and Löfroth[7] were the first to postulate that in fact two types of radical species coexist in sucrose, each located respectively in the glucose and fructose monosaccharide units of sucrose. In later studies,[8] the number of possible sucrose radicals even increased. However, the fact that radicals in the irradiated sucrose crystal may be located on the separate monomer sugars prompted researchers to investigate the EPR characteristics of these sugars in detail. In this light, several studies have investigated irradiated α-glucose and α-Me-glucose by EPR and electron nuclear double resonance (ENDOR).[9] It was only recently that an EPR study was conducted on irradiated solid state β-D-fructose using ENDOR and ENDOR-induced EPR (EI-EPR).[10] This work reports the identification of two dominant radicals indicated as F1 and F2. Both radicals are characterized by three β-type proton hyperfine couplings, as detected by the EI-EPR experiment (see Table 1). This would suggest that the unpaired electron of both fructose radicals interacts with three protons yielding six hydrogen hyperfine tensors. However, only five tensors have been determined with

* To whom all correspondence should be addressed. Fax: 32 9 264 65 60. E-mail: ewald.pauwels@rug.ac.be.
† Laboratory of Theoretical Physics, Ghent University.
‡ European Patent Office.
§ Department of Solid State Sciences, Ghent University.
|| Free University of Brussels.

10.1021/jp0264174 CCC: $22.00
Published on Web 12/02/2002

TABLE 1: Experimental hfcc Values and Direction Cosines of Radicals F1 and F2 as Determined in Ref 10[a]

	experiment					
	A_{iso}	T_{aniso}	A	axes		
F1_β1	96.9	−4.2	92.7	−0.448	−0.253	0.858
		−2.9	94.0	0.675	−0.724	0.139
		7.1	104.0	0.586	0.642	0.495
F1_β2	37.3	−4.1	33.2	−0.476	0.86	0.185
		−2.4	34.9	−0.78	−0.51	0.362
		6.6	43.9	0.406	0.028	0.914
F1_β3	9.3	−3.3	6.0	−0.318	−0.946	−0.066
		−1.7	7.6	−0.225	0.008	0.974
		5.0	14.3	−0.921	0.325	−0.215
F2_β1	87.5	−3.6	83.9	−0.479	−0.365	0.798
		−3.2	84.3	0.642	−0.766	0.035
		6.8	94.3	0.598	0.529	0.601
F2_β2	43.1	−3.9	39.2	−0.262	0.929	0.263
		−2.7	40.4	−0.852	−0.351	0.389
		6.5	49.6	0.453	−0.122	0.883

[a] A_{iso}, T_{aniso}, and A values are in MHz; directions cosines are referred to the *abc* reference axis system of the crystal.

ENDOR, since the missing tensor in F2 probably corresponds with a small hyperfine interaction that could not be determined unambiguously.

Several model fructose radicals can be suggested on the basis of experimental data and theoretical considerations. In this paper, we only retain four model structures that are serious candidates for the observed fructose radicals. Extensive high-level quantum chemical calculations within density functional theory (DFT)[11] have been performed on these four model structures. In addition to its ever-increasing importance in the calculation of molecular ground state properties,[12] DFT has also emerged as a highly suitable method for the calculation of hyperfine coupling tensors provided that hybrid functionals are used and the Kohn−Sham orbitals are expanded in large basis sets. Suitable basis sets are the EPR-II and EPR-III sets specifically designed by Barone for the evaluation of EPR properties in DFT.[13] In this work, it is also pointed out that the best results are obtained with hybrid schemes (B3LYP functional). A relevant study on the adequacy of DFT methods in predicting EPR parameters has been performed by Gauld, Eriksson, and Radom.[14] In this paper, the effects of different basis sets and computational methods on calculated EPR parameters have been extensively investigated. It is concluded that of all DFT approaches, the best accuracy is found with a B3LYP functional for which the results are better than QCID but not as good as QCISD. It should be stressed that the latter method is computationally very demanding and not of practical use in large molecular systems.

It is a great advantage of DFT methods that they are very efficient, and this efficiency is mainly due to its cost effective incorporation of electron correlation by means of its density functional.[13,15] DFT calculations have also been successfully applied for large radical systems such as DNA radicals,[16,17] amino acids,[18] and steroid radicals.[19] These studies have shown the usefulness and feasibility of DFT methods in the calculation of EPR spectroscopic properties of biomolecules, by comparing computed and experimental coupling constants of radicals for which in most cases the probable identity could be proposed. Consequently, simulations were mostly restricted to calculating the hyperfine coupling constants (hfcc values) for the experimentally suggested hypothetical structures.

In this study, we also adopt the single molecule approach to evaluate the model radical structures on their validity. This implies that the crystalline molecular environment surrounding the radical was not incorporated in any way. Calculations on the radical are therefore performed in the (ideal) gas phase, at 0 K. This methodology has been used in several studies and has proven quite successful.[18,19] However, in the gas phase, the radical has more degrees of freedom than it would have in a (simulated) solid state environment. Some of these degrees can then be assessed separately in the search for a conformation that properly reproduces the experimental EPR data. It should be noted that the current single molecule approach has its limitations in the sense that typical geometry effects cannot be modeled due to the complete absence of the local molecular environment surrounding the radical. Crystal matrix effects such as the formation of hydrogen bonds or displacements of atoms are not involved in this approach. Therefore, cluster models are highly appropriate to describe all of these geometry effects and their feasibility and adequacy were recently investigated for the L-α-alanine crystal by Pauwels et al.[20]

Nevertheless, because of the heavy computational burden of cluster model calculations, the single molecule approach has its usefulness in its flexibility to study the effects invoked by switching on different degrees of freedom present in isolated molecules, such as internal rotations. Release of these degrees of freedom can lead to reliable indications of the true physical interpretation of some experimentally observed phenomena. The predictive power of the single molecule approach motivates its use in the investigation of suitable structures for the β-D-fructose radicals.

2. Theoretical Considerations

Because a more detailed description of the theoretical EPR principles can be found in several standard works,[15,21] only the most essential theoretical equations will be discussed briefly. The EPR hyperfine coupling interaction embodies the interaction between the electronic spin and the nuclear spin magnetic moments. This interaction is included in the spin Hamiltonian, which holds all interactions taking place in the molecular system in the presence of a magnetic field. For a paramagnetic system characterized by an electronic spin $S = 1/2$ and nuclear angular moment $I = 1/2$, the general expression for this Hamiltonian can be simplified to

$$H = \beta_e \mathbf{B} \cdot \mathbf{g} \cdot \mathbf{S} - g_n \beta_n \mathbf{I} \cdot \mathbf{B} + \mathbf{S} \cdot \mathbf{A} \cdot \mathbf{I}$$

with β_e the Bohr magneton, β_n the nuclear magneton, and g_n the nuclear magnetogyric ratio. The first two terms in the spin Hamiltonian reflect the electronic and nuclear Zeeman contributions and arise from the interaction of the external magnetic field **B** and the magnetic moments of the electrons and nuclei, specified by **S** and **I**, respectively. In the first Zeeman term, **g** represents the so-called *g*-tensor. The hyperfine interaction matrix **A** in the last term of the spin Hamiltonian is often divided into an isotropic and anisotropic part

$$\mathbf{A} = A_{iso}\mathbf{1} + \mathbf{T}$$

with **1** the 3 × 3 unit matrix. The isotropic part A_{iso} of the hyperfine matrix arises from the coupling between the magnetic moments of the electrons *i* and the nucleus *n* through a contact interaction. It depends solely on the unpaired spin density $\sum_{\mu,\nu} P_{\mu,\nu}^{\alpha-\beta}$ at the position of the nucleus. This is shown in the following equation, assuming that the *g*-tensor is isotropic

$$A_{iso}^{n} = (8\pi/3)\, g\, \beta_e g_n \beta_n \sum_{\mu,\nu} P_{\mu,\nu}^{\alpha-\beta} \langle \varphi_\mu(r_{ni}) |\delta(r_{ni})| \varphi_\nu(r_{ni}) \rangle$$

with φ_μ and φ_ν atomic orbitals centered on nucleus *n*. The

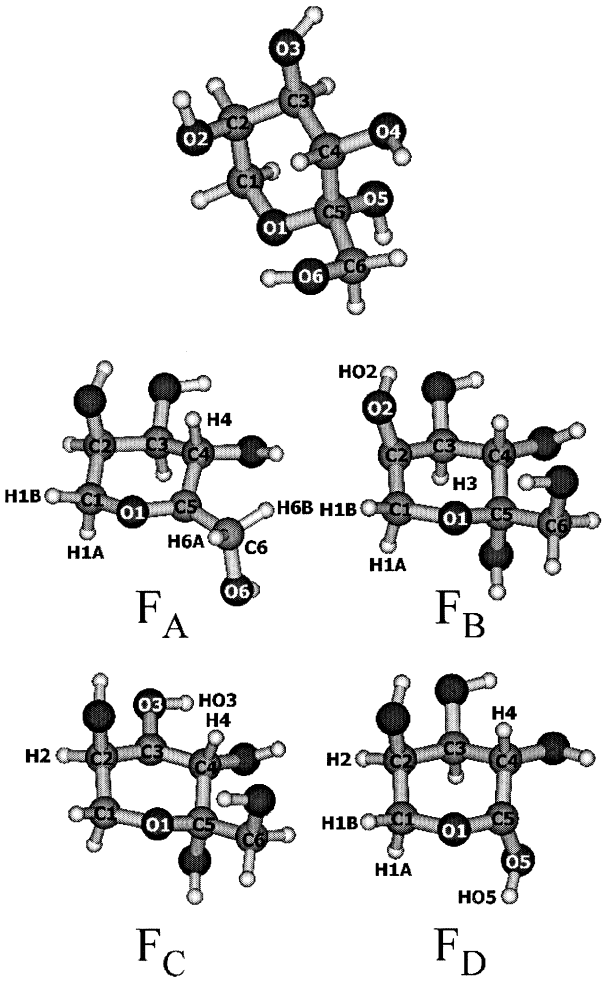

Figure 1. Molecular structure of β-D-fructose as determined by neutron diffraction[20] and the optimized geometries of the proposed model radicals.

anisotropic part of the hyperfine matrix is due to the interaction of magnetic dipoles and is described by the following equation

$$T_{kl}^{n} = g\,\beta_e\,g_n\,\beta_n \sum_{\mu,\nu} P_{\mu,\nu}^{\alpha-\beta} \langle \varphi_\mu(r_{ni}) |r_{ni}^{-5}(r_{ni}^{2}\delta_{kl} - 3r_{ni,k}r_{ni,l})| \varphi_\nu(r_{ni})\rangle$$

for the klth component of the 3×3 anisotropic hyperfine interaction matrix **T**. Diagonalization of this matrix yields the three eigenvalues (or principal components) and corresponding eigenvectors (or principal axes) relative to the reference axis system. In this work, special attention will be paid to the theoretical reproduction of the principal axes of the hyperfine tensor.

3. Model Selection and Computational Details

β-D-Fructose adopts the pyranose form in the crystalline state. Its structure was thoroughly examined by Takagi and Jeffrey in a neutron diffraction study[22] and is visualized in Figure 1. In view of the fact that Vanhaelewyn et al.[10] reported three β-type couplings for both detected radical species, only a limited number of radical structures can be proposed from the undamaged crystal structure of fructose that meet the experimental requirements. Radical models were selected, starting from the assumption that in the process of radiation-induced radical formation, the pyranose ring structure of fructose was preserved. Furthermore, we required the models to be neutral. Starting from these assumptions, all possible homolytic cleavages of the fructose ring substituents had to be considered.

First, we looked at the possible radiation products with an abstracted hydroxyl group. By removing the OH group from carbon atoms C_2 through C_6 in the undamaged molecular structure of fructose, these carbon atoms become radical centers. In the case of C_2, C_3, C_4, and C_6, a structure is generated with one hydrogen directly bound to the carbon carrying the unpaired electron. The hyperfine coupling of this proton would undeniably be visible experimentally as it displays the α-type characteristics. Because both F1 and F2 only display three β-type couplings in the experiment, the aforementioned radiation products can be eliminated. Abstraction of the OH group from C_5 does not yield a structure with an α-type proton but is instead characterized by an unpaired electron that is presumably delocalized over C_5 and O_1. Furthermore, at least three protons are suitably located to produce a β-type coupling with the radical center: the protons of the hydroxy methyl group at C_6, the proton at C_4, and, through the probable delocalization over the ring oxygen, both protons at C_1. Because this structure was potentially consistent with the experimental results, it has been retained as a possible candidate for the experimentally observed radicals (F_A in Figure 1).

A second set of possible radicals is formed with the extraction of a hydrogen from the undamaged β-D-fructose structure. Hydrogen abstraction from C_1 and C_6 yields structures with an α-type proton so these can be eliminated. The radical created by abstracting a hydrogen from C_4 can also be rejected as a possibility, since no three protons can be found that are in a β-position relative to the unpaired electron. The structures with one hydrogen removed from either C_2 or C_3—respectively denoted by F_B and F_C in Figure 1—were further examined in our calculations. Both structures are potentially consistent with the experimental data, since at least three β-type protons can be identified. In F_B, both C_1 protons, the hydroxy proton at O_2, and the proton at C_3 can produce a β-type coupling with the unpaired electron, while in model structure F_C the protons at C_2 and C_4 together with the hydroxy proton at O_3 are in a β-position relative to the unpaired electron.

Finally, a fourth model radical structure was proposed that was generated by homolytic cleavage of the hydroxy methyl group from carbon C_5. This leaves a hydroxy group directly bound to the radical center, which is most probably delocalized over ring oxygen O_1 and carbon C_5. Four possible β-type couplings can be generated in this structure by ring protons H_{1A}, H_{1B} through delocalization of the radical center, ring proton H_4, and by the hydroxy proton H_{O5}. This candidate structure was labeled F_D, and it is also included in Figure 1.

In total, four model radical structures were proposed that could potentially yield EPR parameters in agreement with the experimental results. Extensive calculations were performed on these models to assess the value of each model separately.

The four proposed geometries for the fructose radicals were further refined by optimization in a DFT framework using the B3LYP functional,[23] since several studies [24] have already indicated that this functional reliably describes the geometry of a radical. Molecular orbitals were expanded in a triple-ζ 6-311G basis augmented with single d polarization functions.[25] All calculations were performed with the Gaussian 98 package.[26] Subsequently, isotropic and anisotropic components of the hyperfine tensor were calculated, as well as the associated eigenvectors. This was also done using a B3LYP functional in Gaussian 98. Even though specialized basis sets exist for EPR calculations (such as the EPR-III basis set of Barone[13]), we chose to perform our calculations in a triple-ζ 6-311G basis

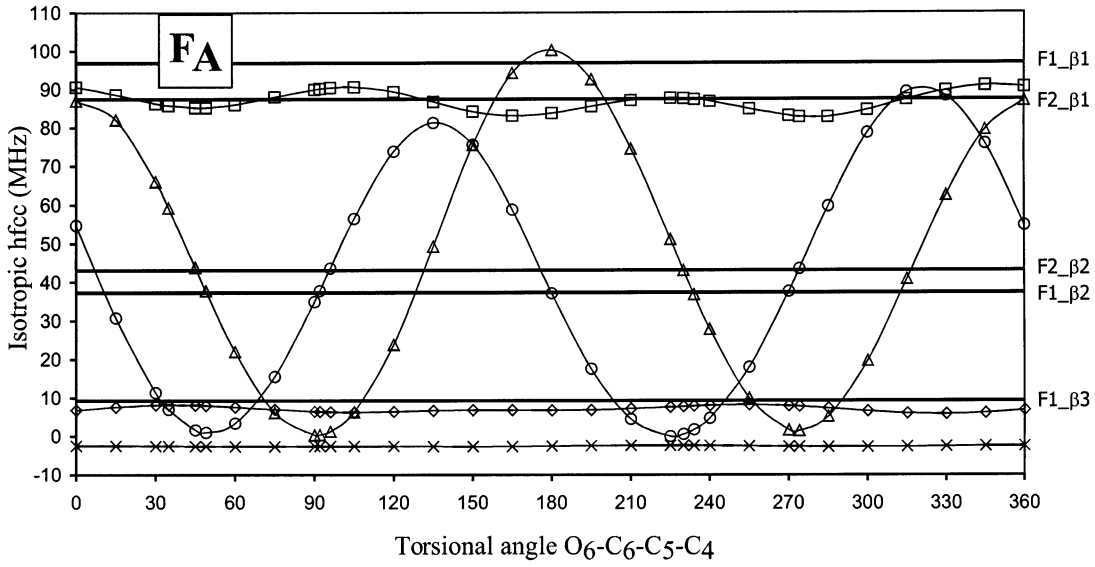

Figure 2. Isotropic proton hfcc values in model radical F_A as a function of the hydroxy methyl group rotation (◇, H_{1A}; ×, H_{1B}; □, H_4; △, H_{6A}; ○, H_{6B}; all other proton hfcc values were close to zero throughout the rotation and are therefore not included). The experimental hfcc values are indicated by thick solid lines.

augmented with single d polarization functions. Representative test calculations with the EPR-III set were performed, but only slight changes in the calculated EPR parameters were observed, despite a substantially larger computational cost. A more detailed discussion on these test calculations will be given in the next section.

4. Results and Discussion

Model Structure F_A. As already noted, the model radical F_A is obtained by removal of the hydroxyl group from the carbon C_5 in the fructose molecule. In the optimized radical structure, the unpaired spin is mainly located at the carbon atom C_5 and to a smaller extent at the oxygen O_1 with respective spin densities of 0.83 and 0.12. We also notice that in the optimized radical geometry the sp^3 hybridization on C_5 is partly retained with respect to the undamaged fructose molecule. This can roughly be verified by the out of plane deviation of the C_5 carbon center, as measured by the angle between the planes through atoms $C_6-C_4-O_1$ and $C_4-O_1-C_5$, respectively. In the fructose molecule, this angle amounts to −37.4°, while in the optimized radical geometry of F_A it reduces to −19.2°.

The most relevant degree of freedom in the single molecule approach of F_A is the internal rotation of the hydroxy methyl group about the C_5-C_6 single bond, characterized by the $O_6-C_6-C_5-C_4$ torsional angle. As this torsional angle will only be fixed in a cluster model calculation due to the formation of hydrogen bonds with the surrounding molecules, we investigated the fluctuation of the isotropic hfcc values of the hydrogen atoms in F_A as a function of the torsional angle $O_6-C_6-C_5-C_4$. This constitutes just the advantage of the single molecule approach: to scan all geometries—allowed by the degrees of freedom—in an attempt to search for specific geometries that are suitable for a fair reproduction of the experimental data. This should allow us to put forward a fairly accurate conformation for the radical in the crystalline state.

The results of the variation of the torsional angle $O_6-C_6-C_5-C_4$ are given in Figure 2. As could be expected, the hydroxy methyl proton hfcc values of H_{6A} and H_{6B} are largely affected by their position. They show a somewhat sinusoidal behavior in function of the torsional angle. The experimentally measured isotropic hfcc values are also displayed in this figure (thick solid lines), and we easily observe that eight conformations may possibly lead to a fair reproduction of the experimental results. We will first compare the theoretical results with the couplings of the experimental F1 species. The large F1_β1 coupling of 96.6 MHz most likely corresponds to the H_4 hfcc, which fluctuates about 90 MHz throughout the rotation of the hydroxy methyl group. The H_{1A} and H_{1B} proton hfcc values remain practically constant during the rotation (roughly 8 and −3 MHz, respectively), but the H_{1B} proton displays a smaller coupling than H_{1A}. If we assign the H_{1A} hfcc to the experimental F1_β3 coupling (9.3 MHz), it is clear that one of the hydroxy methyl proton hfcc values should correspond with the F1_β2 coupling (37.3 MHz) while the other should be close to zero and consequently not be detectable experimentally. Figure 2 reveals that only four conformations succeed in reproducing the three experimental signals of F1 theoretically: (i) a torsional angle of 49° yields an H_{6A} hfcc of 37.8 MHz corresponding with the experimental F1_β2 coupling of 37.3 MHz; (ii) a torsional angle of 92° meets the H_{6B} hfcc of 37.8 MHz with the experimental estimate; (iii) at 234°, a correspondence is found for the H_{6A} hfcc (36.8 MHz), while (iv) at 270° the H_{6B} hfcc yields 37.6 MHz. The four proposed cases all predict an hfcc for the counterpart proton (H_{6A} or H_{6B}) below 6 MHz agreeing with the fact that these signals have not been detected experimentally.

To disentangle between these four proposed conformations, a detailed study was made of the anisotropic components of the calculated hyperfine coupling tensors and their corresponding spatial directions. The anisotropic components of the hyperfine tensor, however, were all in close agreement with the experimental results and did not differ significantly from each other. So, to single out the conformations that correspond with reality, it was necessary to look at the direction cosines of the associated eigenvectors. So far, little or no theoretical studies on organic crystals have used this additional information in the search for a valid structure that reproduces the experimental data.

The three principal axes of the experimental hyperfine tensors are specified by their corresponding direction cosines with respect to the reference frame, which usually coincides with the crystal axes (schematically shown in Figure 3a). The experimental values for the two observed radicals F1 and F2 are reported in Table 1. Because, as stated earlier, the crystalline

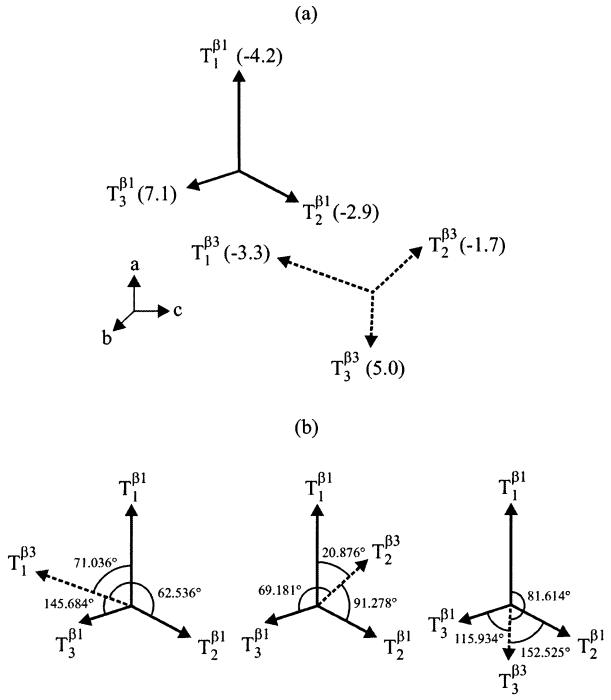

Figure 3. (a) Principal axes of the experimental $\beta 1$ and $\beta 3$ signals as given by their direction cosines with respect to the *abc* reference frame. (b) Displays the mutual angles; the principal axes of the hyperfine tensors are specified by their corresponding anisotropic value (in MHz).

environment was not simulated in the present theoretical calculations, it is impossible to insert the same reference axis system as was done in the experiment. To solve this ambiguity, the mutual angles between the calculated proton tensor axes were compared with the mutual angles between the experimental principal axes of the observed radicals, as shown in Figure 3b for the $\beta 1$ and $\beta 3$ signals in radical F1. In this way, we eliminate the choice of the reference axis system and we obtain an additional reliable tool to differentiate between the four conformations proposed by the theory. It should be stressed that there is still some ambiguity in fixing the relative angles (φ or $\pi-\varphi$) due to the fact that the absolute sign of the experimental direction cosines cannot be determined. This ambiguity was taken into consideration in our analysis of the relative angles, which are reported in Table 2 along with their calculated counterparts. It is found that the angles between the principal axes, calculated for the conformation at 234° are in close agreement with the angles between the experimental F1 signals. The other conformations do not succeed by far in reproducing the experimental findings. It should be noted, however, that the smallest two anisotropic components for the H_4 proton have been switched to allow for a fair comparison. This means that for the conformation at 234°, the eigenvector for the −2.0 MHz anisotropic component of H4 matches with the eigenvector of the −4.2 MHz experimental component of F1 and likewise the −5.3 MHz eigenvector of H_4 matches with the −2.9 MHz F1 experimental component. This interchange is not dramatic and is supported by a theoretical analysis of the angles formed by the H_4 principal axes with those of the two other protons H_{6A} and H_{1A}. The reason for this switch between the two low anisotropic component axes can be attributed to the fact that the present calculations did not involve any simulation of the molecular environment, but this should unambiguously be affirmed by additional cluster calculations. Apart from this interchange, all anisotropic and isotropic proton hyperfine couplings in experimental species F1 are in close agreement with the coupling values in model radical F_A, as summarized in Table 3. The fair reproduction of the mutual angles between the anisotropic principal axes strengthens the identification of the experimental species F1 as having a radical structure conform model F_A and with a hydroxy methyl torsional angle of 234° for $O_6-C_6-C_5-C_4$. An additional calculation was performed on this conformation to assess the choice of the basis set used in the calculation of the EPR parameters. EPR parameters calculated with an (extended) EPR-III basis, which has been constructed by Barone for specific use in this field,[13] are compared to those obtained with a 6-311G* basis (Table 3). We notice only small discrepancies, apart from the H_4 coupling, which is substantially higher in the (EPR-III) large basis and is in fact in much better agreement with the experimental $\beta 1$ hfcc (Table 1). The anisotropic principal values are nearly identical for both basis sets, and the relevant principal directions diverge with a maximum of some 4°. So, only for the isotropic hyperfine couplings, a better agreement with experimental data is obtained for the EPR-III basis. However, because the hfcc values of H6A and H6B change only in a minor way with respect to the 6-311G* calculation, the use of a larger basis set has no effect on the final identification of the hydroxy methyl torsional angle at 234°.

The experimental F2 species also shows three β-type couplings in the EI-EPR spectrum that are very similar to the first F1 species. However, only two β-type couplings could be determined unambiguously with ENDOR. From Figure 2, it is clear that the experimental isotropic hfcc values of F2 are reproduced at four possible conformations of F_A, differing from the previous four conformations by only a small fraction of the hydroxy methyl torsional angle (about 4°). This minor difference is due to the extreme sensitivity of the isotropic hfcc values for slight changes in the relative position of the hydroxy methyl protons with respect to the unpaired spin density on the sp^3-like lobe of C_5. A study of the anisotropic hyperfine eigenvectors is again required to disentangle the four conformations. In F2, however, only the mutual angles between the $\beta 1$ and the $\beta 2$ anisotropic components are available for comparison with calculated results (also taken up in Table 2). In addition, there is a striking resemblance between these values and those between the $\beta 1$ and the $\beta 2$ signals in radical F1. This indicates that the F2 conformation is very similar to the F1 conformation. A detailed investigation of the experimental data reveals that the difference in spatial direction of the observed anisotropic components is very small (Table 4) and almost all are of the same magnitude for $\beta 1$ and $\beta 2$. Because of the missing $\beta 3$ signal in F2, there is insufficient ground to make an essential difference between the two experimentally observed F1 and F2 species and we sustain the conclusion that both exhibit the same radical structure according to the proposed F_A configuration but with slightly altered conformations.

Model Structures F_B and F_C. By hydrogen abstraction from C_2 and C_3, respectively, the model radicals F_B and F_C are formed. In both optimized radical geometries, the unpaired electron is predominantly located on the carbon atoms—C_2 and C_3 have spin densities of 0.80 and 0.81, respectively—but is to some extent delocalized over the attached oxygen atoms O_2 and O_3 with respective spin densities of 0.15 and 0.13. Both optimized radical geometries display a carbon radical center that retains its original sp^3 hybridization for the larger part. In F_B, C_2 has an out of plane deviation of 23.3° vs 34.7° in the crystal, as measured by the angle between the planes $O_2-C_3-C_1$ and $C_3-C_1-C_2$. The radical center in F_C is also far from planar

TABLE 2: Comparison of the Angles between the Calculated Principal Axes of F_A Proton Hyperfine Tensors (Calculated for a Torsional Angle of 234°) and the Angles between Their Experimental Counterparts

Experiment

			F1_β1		
	A_{iso}		96.9		
		T_{aniso}	-4.2	-2.9	7.1
		-3.3	71.0	62.5	145.7
F1_β3	9.3	-1.7	20.9	91.3	69.2
		5.0	81.6	152.5	115.9

			F1_β1		
	A_{iso}		96.9		
		T_{aniso}	-4.2	-2.9	7.1
		-4.1	81.1	156.7	68.6
F1_β2	37.3	-2.4	37.9	96.1	127.2
		6.6	53.5	67.6	44.9

			F1_β2		
	A_{iso}		37.3		
		T_{aniso}	-4.1	-2.4	6.6
		-3.3	132.4	45.0	102.4
F1_β3	9.3	-1.7	72.9	58.4	37.0
		5.0	47.3	61.6	124.1

			F2_β1		
	A_{iso}		87.5		
		T_{aniso}	-3.6	-3.2	6.8
		-3.9	90.2	150.5	60.5
F2_β2	43.1	-2.7	32.1	105.3	117.5
		6.5	57.8	65.5	42.5

Theory

			H4		
	A_{iso}		87.4		
		T_{aniso}	-2.0	-5.3	7.3
		-4.3	84.2	75.4	164.3
H1A	7.9	-2.9	10.1	83.4	82.3
		7.2	81.7	164.0	103.6

			H4		
	A_{iso}		87.4		
		T_{aniso}	-2.0	-5.3	7.3
		-4.7	76.4	126.0	39.3
H6A	36.8	-3.0	35.4	108.3	119.1
		7.7	58.1	41.8	66.1

			H6A		
	A_{iso}		36.8		
		T_{aniso}	-4.7	-3.0	7.7
		-4.3	125.0	51.0	121.6
H1A	7.9	-2.9	66.2	39.3	60.7
		7.2	44.5	86.0	134.2

TABLE 3: Summary of Calculated Proton Hyperfine Tensor Components for the F_A Conformation with a Torsional Angle of 234°[a]

	conformation at 234°							
	6-311G*			EPR-III				experimental
	A_{iso}	T_{aniso}	A	A_{iso}	T_{aniso}	A	$\Delta_{direction}$	match
H1A	7.9	−4.3	3.6	8.5	−4.4	4.1	1.489	F1_β3
		−2.9	5.0		−2.7	5.8	1.495	
		7.2	15.1		7.1	15.6	0.172	
H1B	−2.4	−3.1	−5.5	−2.7	−3.0	−5.7	5.348	
		−2.6	−5.0		−2.5	−5.2	5.352	
		5.7	3.3		5.6	2.9	0.183	
H4	87.4	−2.0	85.4	94.9	−2.2	92.7	3.656	F1_β1
		−5.3	82.1		−5.2	89.7	3.652	
		7.3	94.7		7.4	102.3	0.343	
H6A	36.8	−4.7	32.1	39.5	−4.8	34.7	1.002	F1_β2
		−3.0	33.8		-2.9	36.6	1.026	
		7.7	44.5		7.7	47.2	0.212	
H6B	1.7	−5.1	−3.4	2.0	−5.3	−3.3	4.972	
		−4.0	−2.3		−4.0	−2.0	4.978	
		9.1	10.8		9.3	11.3	0.285	

[a] The A_{iso}, T_{aniso}, and A values (in MHz) are reported for a 6-311G* and an EPR-III basis. No direction cosines are given, but anisotropic values are ordered in comparison with their experimental counterparts in Table 1. $\Delta_{direction}$ is the difference (in degrees) between the anisotropic principal axes calculated with both basis sets.

TABLE 4: Angles between Corresponding Principal Axes for both β1 and β2 Tensors in Experimental Radicals F1 and F2; A_{iso} and T_{aniso} Values Are in MHz

	F1_β1			F1_β2		
A_{iso}	96.6			37.3		
T_{aniso}	−4.2	−2.9	7.1	−4.1	−2.4	6.6
angle	7.5	6.7	8.9	13.7	10.1	9.2
T_{aniso}	−3.6	−3.2	6.8	−3.9	−2.7	6.5
A_{iso}	87.5			43.1		
	F2_β1			F2_β1		

with an angle of 20.5° between the planes $O_3-C_4-C_2$ and $C_4-C_2-C_3$ vs 33.9° in the crystal.

Because in both F_B and F_C the radical center is not located near the hydroxy methyl group, rotation about the C_5-C_6 axis has little or no effect on the spin density distribution throughout the radicals and consequently on the proton hfcc values. This degree of freedom can therefore be totally eliminated. On the other hand, rotation of the hydroxy group about the C_2-O_2 and C_3-O_3 axes in F_B and F_C, respectively, does influence the spin density distribution. The isotropic hfcc values of the principal protons are therefore plotted in Figure 4 as a function of these degrees of freedom. Both plots display a striking similarity for the hfcc values of the hydroxy protons (H_{O2} and H_{O3}) as a function of hydroxy group rotation. The two large maxima in each plot are encountered when the hydroxy proton is either coplanar or antiperiplanar to the orbital containing the unpaired electron. The asymmetry in both maxima is due to the nonplanarity of the radical center, and the largest maximum is found when the hydroxyproton is antiperiplanar to the partial sp^3 lobe of the orbital with the unpaired electron. While in only two conformations of model radical F_B, the experimental results are possibly reproduced, and model radical F_C has eight possible conformations.

In F_B, three proton hfcc values vary significantly upon rotation of the hydroxy group. The hfcc values of H_{1A}, H_{O2}, and H_3 show a sinusoidal pattern, while that of H_{1B} remains practically constant throughout the rotation. In the search for a conformation that possibly reproduces the experimental results, H_3 most likely can account for the β2 signals in both F1 and F2, and H_{1A} can be associated with the β3 signal in F1. However, because H_{1A} becomes rather large (up to 30 MHz) at some conformations, only the region between 300 and 360° seems acceptable. In this

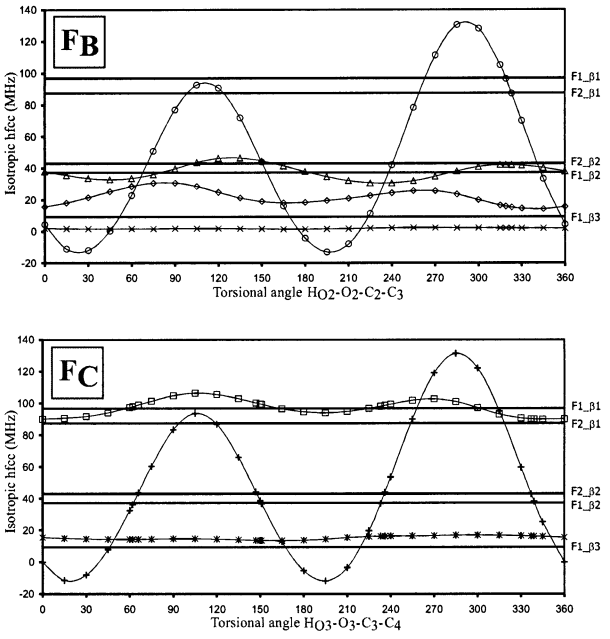

Figure 4. Isotropic proton hfcc values in model radicals F_B and F_C as a function of the hydroxy group rotation (◇, H_{1A}; ×, H_{1B}; *, H_2; ○, H_{O2}; △, H_3; +, H_{O3}; □, H_4; all other proton hfcc values were close to zero throughout the rotation and are therefore not included). The experimental hfcc values are indicated by thick solid lines.

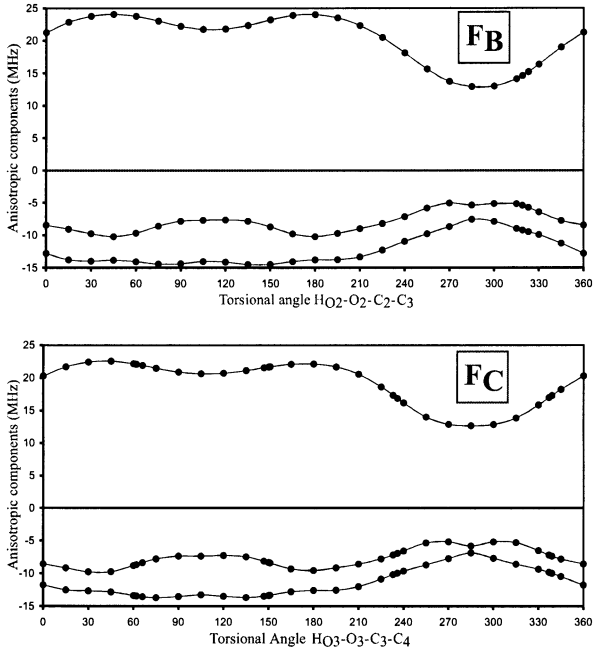

Figure 5. Anisotropic components of hydroxy proton hyperfine tensors in model radicals F_B and F_C as a function of the hydroxy group rotation.

interval, the conformation at 319° displays a H_{O2} hfcc in accordance with the β1 signal of the experimentally observed F1 radical. Even though experimentally no F2_β3 signal was quantitatively detected, Vanhaelewyn et al.[10] report a third hyperfine coupling for F2 similar to the β3 coupling in F1. It is therefore safe to assume that a conformation in accordance with F2 must be searched for in the same region between 300 and 360°. At a $H_{O3}-O_3-C_3-C_4$ torsional angle value of 323°, a conformation is found that conclusively exhibits an H_{O2} hfcc in close agreement with the β1 signal of the F2 radical.

The model radical F_C only has three protons with significant hfcc values. The H_4 proton hfcc corresponds with the β1 signals of F1 and F2 and fluctuates around 100 MHz. The hfcc of H_2 remains more or less constant throughout the hydroxy group rotation and accords with the β3 signal of F1. At four conformations—with $H_{O3}-O_3-C_3-C_4$ torsional angles of 62, 151, 233, and 339°—the H_{O3} hfcc accords with the F1_β2 signal. Similarly, four conformations can be found that have an H_{O3} hfcc in agreement with the F2_β2 signal—at 66, 147, 236, and 337°.

However, particularly large anisotropic components for the hydroxy proton hyperfine tensors in all conformations of both F_B and F_C instructed us to further examine these components. Figure 5 shows the variation of the anisotropic hydroxy proton components as a function of the hydroxy group rotation. The largest component in both charts fluctuates at 20−25 MHz and only drops to 12−13 MHz in the region where the hydroxy proton is antiperiplanar to the unpaired electron sp^3 orbital. Similarly, the smaller anisotropic components display couplings of −10 and −15 MHz, respectively, and rise to −5 and −7 MHz in the antiperiplanar region. Comparison with the experimental anisotropic components in Table 1 clearly shows that the theoretical predictions are far too high. Even in conformations where the hydroxy proton is more or less antiperiplanar to the unpaired electron orbital, the predicted anisotropic components are roughly twice the experimental values. This is most likely due to the high spin density on the hydroxy group oxygen, which assigns the hydroxy proton with some α-proton character.

Despite the large anisotropic components, a number of conformations of both F_B and F_C were further analyzed on the basis of the hyperfine coupling tensor direction cosines. The F_B conformations with a $H_{O2}-O_2-C_2-C_3$ torsional angle of 319 and 323° were examined, as were the F_C conformations at 233, 236, 337, and 339° for the $H_{O3}-O_3-C_3-C_4$ torsional angle. In all of these conformations, the hydroxy proton is more or less antiperiplanar to the unpaired electron orbital and the hydroxy proton anisotropic components bear at least some resemblance with the experimental components. However, evaluation of the mutual angles between the calculated proton tensor components and the angles between the experimental tensor components led to no comparison at all. For no conformation, theoretical angles were obtained that were in agreement with the experimental ones. This fact, together with the overestimated anisotropic components, led us to the conclusion that model radicals F_B and F_C are not realistic models for the experimental radicals F1 and F2.

Model Structures F_D. F_D is the smallest of all model radicals examined and is created by abstraction of the hydroxy methyl group from (undamaged) fructose. The unpaired spin is mainly located on the C_5 carbon atom with a spin density of 0.80 but is to some extent delocalized to the O_5 atom (0.12 spin density). Surprisingly, little or no spin density resides on the ring oxygen O_1, in contrast with the ring oxygen in model radical F_A, where the unpaired electron was also mainly located on C_5 but partially delocalized to O_1. This is probably due to the large sp^3 hybridization character of the C_5 radical center in F_D. The out of plane deviation of the radical center C_5, as expressed by the angle between the planes $O_5-C_4-O_1$ and $C_4-O_1-C_5$, is 24.7° in the model radical vs 34.5° in the fructose crystal.

As was the case in F_B and F_C, the hydroxy group rotation is the relevant degree of freedom that must be examined in the search for a conformation that suitably reproduces the experimental data. In Figure 6, the significant proton hfcc values are plotted as a function of the rotation of the hydroxy group about the O_5-C_5 axis (as expressed by the torsional angle $H_{O5}-O_5-$

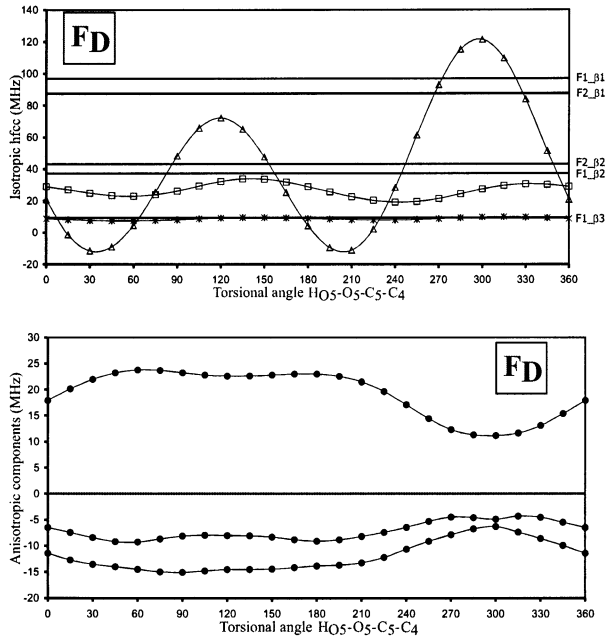

Figure 6. Isotropic hfcc values and H_{O5} hydroxy proton anisotropic hyperfine tensor components in model radical F_D as a function of the hydroxy group rotation (*, H_2; □, H_4; △, H_{O5}; all other proton hfcc values were close to zero throughout the rotation and are therefore not included). The experimental hfcc values are indicated by thick solid lines.

C_5-C_4). Surprisingly, the H_2 proton yields a considerable hfcc of about 10 MHz throughout the hydroxy group rotation, while the H_{1A} and H_{1B} protons do not generate substantial isotropic hfcc values. These proton couplings amount to −3 MHz at best, and they were therefore not included in Figure 6. This is altogether quite remarkable since the H_{1A} and H_{1B} protons are in a γ-position with respect to the radical center at C_5, while the H_2 proton is in a δ-position. So, only three protons produce a significant hfcc, which can be matched with the experimental values. The H_2 proton hfcc is in accordance with the F1_β3 signal throughout the plot, and conformations can be found (for instance, at about 270 and 320°) where the H_{O5} proton hfcc could correspond with the β1 coupling of either F1 or F2. The H_4 proton hfcc, however, fluctuates at about 25 MHz, which is quite small in comparison with the experimental F1_β2 and F2_β2 isotropic couplings (37.3 and 43.10 MHz, respectively). In addition, we found that the anisotropic components of the H_{O5} proton hyperfine tensor are far too large in comparison with β1. In Figure 6, a plot of these components is also presented as a function of the hydroxy group torsional angle. The similarity with both charts in Figure 5 is obvious. As a result, no further analysis of the hyperfine tensor eigenvectors was conducted and it was concluded that model radical F_D is not consistent with the experimental results.

5. Conclusions

In this study, single molecule DFT calculations were used to identify the structure of the radiation-induced radicals in solid state β-D-fructose. Four tentative structures were proposed—model radicals F_A, F_B, F_C, and F_D—and EPR calculations were performed on the optimized geometries. In all four model radicals, the main degrees of freedom—rotation of the hydroxy methyl group or hydroxy group—were selectively varied and isotropic hfcc values were recalculated at each point. From these plots, insight was gained on the conformations of which hfcc values were in possible accordance with the experimental values. Analysis of the anisotropic hyperfine tensor components for all significant protons conclusively led to the elimination of model radicals F_B, F_C, and F_D. The relevant anisotropic components in model radical F_A were however in close agreement with experiment.

Subsequently, four possible F_A conformations were selected with isotropic and anisotropic hfcc values that conform to the experimental values of radical species F1. On the basis of the analysis of the tensor direction cosines of these four conformers, one structure was identified that closely matched the experimental direction cosines. The EPR parameters of this conformation, with a torsional angle $O_6-C_6-C_5-C_4$ of 234°, correspond quite accurately with those of the experimental F1 radical species, for both the isotropic and the anisotropic hyperfine components as well as for the directions of the principal axes.

By comparison of the experimental information on the spatial orientation of the measured hyperfine axes between the two radical species F1 and F2, this study is not able to differentiate both and sustains the conclusion that the F1 and F2 species are in fact manifestations of the same radical, with a structure conform F_A but with slightly altered conformations. To further assess this difference, four conformations were examined, which were in close accordance with the F2 experimental data, for both the isotropic and the anisotropic hfcc values. However, because of the high sensitivity of the isotropic hydroxy methyl proton hfcc values for small changes of the $O_6-C_6-C_5-C_4$ torsional angle, these conformers are very close to the previous conformers associated with F1, which is not surprising. On the basis of the experimental isotropic values, only minor conformational changes are found (about 4°), which are not of that extent to further differentiate between radical species F1 and F2, based on the single molecule approach. Part of the experimental information gets lost in this approach since crystal axes are not involved in the model. Translational and rotational degrees of freedom of the radical within the crystal lattice are not addressed, and possible vibrational averaging effects related to pyramidal inversion at the radical center[17] are not taken into account. We conclude that both radical species F1 and F2, found in the experiments of Vanhaelewyn et al.,[10] can be identified as having the radical structure F_A, possibly with a $O_6-C_6-C_5-C_4$ torsional angle at about 234°.

Because the absence of a reference axis system introduces an ambiguity in the above results, further calculations are necessary to make a clear distinction between F1 and F2 in relation to their conformations. This will shortly be verified in extended cluster calculations, where the anisotropic hyperfine eigenvectors can be evaluated relative to the crystal axes.

Acknowledgment. This work is supported by the Fund for Scientific Research—Flanders (FWO) and the Research Board of the Ghent University. G.V. is a Postdoctoral Fellow of the Fund for Scientific Research—Flanders.

References and Notes

(1) CEN/TC 275/WG 8 N 48 Food Analysis—Horizontal Methods—Irradiated Foodstuffs. Secretariat: DIN, Germany. CEN/CS 1995.

(2) CEN/TC 275/WG 8 N 49 Food Analysis—Horizontal Methods—Irradiated Foodstuffs. Secretariat: DIN, Germany. CEN/CS 1995.

(3) (a) Fattibene, P.; Duckworth, T. L.; Desrosiers, M. F. *Appl. Radiat. Isot.* **1996**, *47*, 1375. (b) Nakajima, T.; Otsuki, T.; Hara, H.; Nishiwaki, Y.; Matsuoka, M. *Radiat. Prot. Dosim.* **1990**, *34*, 303. (c) Tchen, A.; Greenstock, C. L.; Trivedi, A. *Radiat. Prot. Dosim.* **1993**, *46*, 119.

(4) (a) Bardsley, J.; Baugh, P. J.; Phillips, G. O. *J. Chem. Soc., Perkin Trans. 2* **1975**, 614. (b) Gilbert, B. C.; King, D. M.; Thomas, C. B. *J. Chem. Soc., Perkin Trans. 2* **1983**, *5*, 675. (c) Triolet, J.; Thiery, C.; Agnel, J. P.; Battesti, C.; Raffi, J.; Vincent, P. *Free Radical Res. Commun.* **1990**, *10*, 57. (d) Triolet, J.; Thiery, C.; Battesti, C.; Agnel, J. P.; Raffi, J.; Vincent,

P. *J. Chim. Phys. Phys. Chim. Biol.* **1991**, *88*, 1237. (e) Triolet, J.; Raffi, J.; Agnel, J. P.; Battesti, C.; Thiery, C.; Vincent, P. *Magn. Reson. Chem.* **1992**, *30*, 1051. (f) Triolet, J.; Thiery, C.; Agnel, J. P.; Battesti, C.; Raffi, J.; Vincent, P. *Free Radical Res. Commun.* **1992**, *16*, 183.

(5) Derouane, E. G.; Vedrine, J. C. *Chem. Phys. Lett.* **1974**, *29*, 222.

(6) (a) Shields, H.; Hamrick, P. *J. Chem. Phys.* **1962**, *37*, 202. (b) Lomaglio, G. C. R. *Seances Acad. Sci. B* **1967**, *264*, 1637.

(7) Gräslund, A.; Löfroth, G. *Acta Chem. Scand. B* **1975**, *29*, 475.

(8) (a) Sagstuen, E.; Lund, A.; Awadelkarim, O.; Lindgren, M.; Westerling, J. *J. Phys. Chem.* **1986**, *90*, 5584. (b) Vanhaelewyn, G.; Sadlo, J.; Callens, F.; Mondelaers, W.; De Frenne, D.; Matthys, P. *Appl. Radiat. Isot.* **2000**, *52*, 1221.

(9) (a) Madden, K. P.; Bernhard, W. A. *Radiat. Res.* **1977**, *70*, 613. (b) Madden, K. P.; Bernhard, W. A. *J. Chem. Phys.* **1979**, *70*, 2431. (c) Madden, K. P.; Bernhard, W. A. *J. Phys. Chem.* **1979**, *83*, 2643. (d) Madden, K. P.; Bernhard, W. A. *J. Chem. Phys.* **1980**, *72*, 31. (e) Madden, K. P.; Bernhard, W. A. *J. Phys. Chem.* **1980**, *84*, 1712. (f) Madden, K. P.; Bernhard, W. A. *J. Phys. Chem.* **1982**, *86*, 4033. (g) Thiery, C. J.; Agnel, J. L.; Frejaville, C. M.; Raffi, J. J. *J. Phys. Chem.* **1983**, *87*, 4485.

(10) Vanhaelewyn, G.; Lahorte, P.; De Proft, F.; Mondelaers, W.; Geerlings, P.; Callens, F. *Phys. Chem. Chem. Phys.* **2001**, *3*, 1729.

(11) For an example of a reference work, see Parr, R. G.; Yang, W. *Density-Functional Theory of Atoms and Molecules*; Oxford University Press: New York, 1989.

(12) (a) Geerlings, P.; De Proft, F.; Langenaeker, W. *Adv. Quantum Chem.* **1999**, *33*, 303. (b) Koch, W.; Holthausen, M. C. *A Chemist's Guide to Density Functional Theory*; Wiley-VCH: Weinheim, 2001.

(13) Barone, V. In *Recent Advances in Density Functional Methods, Part I*; Chong, D. P., Ed.; World Scientific Publishing Co.: Singapore, 1995; Chapter 8.

(14) Gauld, J. W.; Eriksson, L. A.; Radom, L. *J. Phys. Chem. A* **1997**, *101*, 1352.

(15) Malkin, V. G.; Malkina, O. L.; Eriksson, L. A.; Salahub, D. R. In *Modern Density Functional Theory: A Tool for Chemistry*; Pulitzer, P., Seminario, J. M., Eds.; Elsevier: Amsterdam, 1995; Chapter 9.

(16) For some representative studies in this field, see (a) Wetmore, S. D.; Boyd, R. J.; Eriksson, L. A. *J. Phys. Chem. B* **1998**, *102*, 7674. (b) Wetmore, S. D.; Boyd, R. J.; Eriksson, L. A. *J. Phys. Chem. B* **1998**, *102*, 9332. (c) Wetmore, S. D.; Boyd, R. J.; Eriksson, L. A. *J. Phys. Chem. B* **1998**, *102*, 10602.

(17) For some representative studies in this field, see (a) Adamo, C.; Heitzmann, M.; Meilleur, F.; Rega, N.; Scalmani, G.; Grand, A.; Cadet, J.; Barone, V. *J. Am. Chem. Soc.* **2001**, *123*, 7113. (b) Jolibois, F.; Cadet, J.; Grand, A.; Subra, R.; Rega, N.; Barone, V. *J. Am. Chem. Soc.* **1998**, *120*, 1864.

(18) (a) Ban, F.; Wetmore, S. D.; Boyd, R. J. *J. Phys. Chem. A* **1999**, *103*, 4303. (b) Ban, F.; Gauld, J. W.; Boyd, R. J. *J. Phys. Chem. A* **2000**, *104*, 5080. (c) Ban, F.; Gauld, J. W.; Boyd, R. J. *J. Phys. Chem. A* **2000**, *104*, 8583. (d) Himo, F.; Eriksson, L. A. *J. Chem. Soc., Perkins Trans. 2* **1998**, *2*, 305. (e) Lahorte, P.; De Proft, F.; Vanhaelewyn, G.; Masschaele, B.; Cauwels, P.; Callens, F.; Geerlings, P.; Mondelaers, W. *J. Phys. Chem. A* **1999**, *103*, 6650. (f) Rega, N.; Cossi, M.; Barone, V. *J. Am. Chem. Soc.* **1997**, *119*, 12962. (g) Rega, N.; Cossi, M.; Barone, V. *J. Am. Chem. Soc.* **1998**, *120*, 5723.

(19) Lahorte, P.; De Proft, F.; Callens, F.; Geerlings, P.; Mondelaers, W. *J. Phys. Chem. A* **1999**, *103*, 11130.

(20) Pauwels, E.; Van Speybroeck, V.; Lahorte, P.; Waroquier, M. *J. Phys. Chem. A* **2001**, *105*, 8794.

(21) (a) Atherton, N. M. *Principles of Electron Spin Resonance*; Ellis Horwood, Prentice Hall: New York, 1993. (b) Weil, J. A.; Bolton, J. R.; Wertz, J. E. *Electron Paramagnetic Resonance: Elementary Theory and Practical Applications*; Wiley-Interscience: New York, 1994.

(22) (a) Takagi, S.; Jeffrey, G. A. *Acta Crystallogr. B* **1977**, *33*, 3510. (b) Takagi, S.; Jeffrey, G. A. *Acta Crystallogr. B* **1978**, *34*, 1048.

(23) Becke, A. D. *J. Chem. Phys.* **1996**, *104*, 1040.

(24) (a) Wong, M. W.; Radom, L. *J. Phys. Chem. A* **1998**, *102*, 2237. (b) Parker, C. L.; Cooksy, A. L. *J. Phys. Chem. A* **1998**, *102*, 6186. (c) Smith, D. M.; Nicolaides, A.; Golding, B. T.; Radom, L. *J. Am. Chem. Soc.* **1998**, *120*, 10223. (d) Lynch, B. J.; Fast, P. L.; Harris, M.; Truhlar, D. G. *J. Phys. Chem. A* **2000**, *104*, 4811. (e) Van Speybroeck, V.; Van Neck, D.; Waroquier, M.; Wauters, S.; Saeys, M.; Marin, G. B. *J. Phys. Chem. A* **2000**, *104*, 10939.

(25) (a) Krishnan, R.; Binkley, J. S.; Seeger, R.; Pople, J. A. *J. Chem. Phys.* **1980**, *72*, 650. (b) McLean, A. D.; Chandler, G. S. *J. Chem. Phys.* **1980**, *72*, 5639.

(26) Frisch, M. J.; Trucks, G. W.; Schlegel, H. B.; Scuseria, G. E.; Robb, M. A.; Cheeseman, J. R.; Zakrzewski, V. G.; Montgomery, J. A., Jr.; Stratmann, R. E.; Burant, J. C.; Dapprich, S.; Millam, J. M.; Daniels, A. D.; Kudin, K. N.; Strain, M. C.; Farkas, O.; Tomasi, J.; Barone, V.; Cossi, M.; Cammi, R.; Mennucci, B.; Pomelli, C.; Adamo, C.; Clifford, S.; Ochterski, J.; Petersson, G. A.; Ayala, P. Y.; Cui, Q.; Morokuma, K.; Malick, D. K.; Rabuck, A. D.; Raghavachari, K.; Foresman, J. B.; Cioslowski, J.; Ortiz, J. V.; Stefanov, B. B.; Liu, G.; Liashenko, A.; Piskorz, P.; Komaromi, I.; Gomperts, R.; Martin, R. L.; Fox, D. J.; Keith, T.; Al-Laham, M. A.; Peng, C. Y.; Nanayakkara, A.; Gonzalez, C.; Challacombe, M.; Gill, P. M. W.; Johnson, B. G.; Chen, W.; Wong, M. W.; Andres, J. L.; Head-Gordon, M.; Replogle, E. S.; Pople, J. A. *Gaussian 98*, revision A.7; Gaussian, Inc.: Pittsburgh, PA, 1998.